

**Key Points:**

- Compared to Saildrone wind speeds, the ERA-5 reanalysis appears to underestimate the highest wind speed events ( $>10 \text{ m s}^{-1}$ )
- Co-located ocean  $p\text{CO}_2$  and wind speed observations result in larger uptake of  $\text{CO}_2$  in this region by 9%
- Using a sea-state dependent gas transfer velocity leads to a 28% greater ocean uptake of  $\text{CO}_2$  compared to using a wind-only equation

**Supporting Information:**

Supporting Information may be found in the online version of this article.

**Correspondence to:**

S. Nickford,  
sarah\_nickford@uri.edu

**Citation:**

Nickford, S., Palter, J. B., & Mu, L. (2024). The importance of contemporaneous wind and  $p\text{CO}_2$  measurements for regional air-sea  $\text{CO}_2$  flux estimates. *Journal of Geophysical Research: Oceans*, 129, e2023JC020744. <https://doi.org/10.1029/2023JC020744>

Received 22 NOV 2023

Accepted 10 MAY 2024

**Author Contributions:**

**Conceptualization:** S. Nickford, J. B. Palter

**Data curation:** S. Nickford

**Formal analysis:** S. Nickford, J. B. Palter, L. Mu

**Funding acquisition:** S. Nickford, J. B. Palter

**Investigation:** S. Nickford, J. B. Palter, L. Mu

**Methodology:** S. Nickford, J. B. Palter

**Project administration:** J. B. Palter

**Software:** S. Nickford

**Supervision:** J. B. Palter

**Visualization:** S. Nickford, L. Mu

**Writing – original draft:** S. Nickford

**Writing – review & editing:** S. Nickford, J. B. Palter, L. Mu

# The Importance of Contemporaneous Wind and $p\text{CO}_2$ Measurements for Regional Air-Sea $\text{CO}_2$ Flux Estimates

S. Nickford<sup>1</sup> , J. B. Palter<sup>1</sup> , and L. Mu<sup>1,2</sup> 

<sup>1</sup>Graduate School of Oceanography, University of Rhode Island, Narragansett, RI, USA, <sup>2</sup>Cooperative Institute for Climate, Ocean and Ecosystem Studies, College of the Environment, University of Washington, Seattle, WA, USA

**Abstract** Few observational platforms are able to sustain direct measurements of all the key variables needed in the bulk calculation of air-sea carbon dioxide ( $\text{CO}_2$ ) exchange, a capability newly established for some Uncrewed Surface Vehicles (USVs). Western boundary currents are particularly challenging observational regions due to strong variability and dangerous sea states but are also known hot spots for  $\text{CO}_2$  uptake, making air-sea exchange quantification in this region both difficult and important. Here, we present new observations collected by Saildrone USVs in the Gulf Stream during the winters of 2019 and 2022. We compared Saildrone data across co-located vehicles and against the Pioneer Array moorings to validate the data quality. We explored how  $\text{CO}_2$  flux estimates differ when all variables needed to calculate fluxes from the bulk formulas are simultaneously measured on the same platform, relative to the situation where in situ observations must be combined with publicly-available data products. We systematically replaced variables in the bulk formula with those often used for local and regional flux estimates. The analysis revealed that when using the ERA-5 reanalysis wind speed in place of in situ observations, the ocean uptake of  $\text{CO}_2$  is underestimated by 8%; this underestimate grows to 9% if the NOAA Marine Boundary Layer atmospheric  $\text{CO}_2$  product and ERA-5 significant wave height are also used in place of in situ observations. Overall our findings point to the importance of collecting contemporaneous observations of wind speed and ocean  $p\text{CO}_2$  to reduce biases in estimates of regional  $\text{CO}_2$  flux, especially during high wind events.

**Plain Language Summary** The North Atlantic Ocean absorbs a large amount of carbon dioxide ( $\text{CO}_2$ ) from the atmosphere. The ocean  $\text{CO}_2$  uptake mainly occurs during the winter months in a region where a swift ocean current, called the Gulf Stream, carries warm waters from the tropics to northern latitudes.

Understanding how much  $\text{CO}_2$  this ocean region absorbs is important for constraining global scale assessments of the sources and sinks of  $\text{CO}_2$ . In this paper, we reflect on the methods that are typically used to calculate the exchange of  $\text{CO}_2$  between the ocean and atmosphere. Using new data collected by uncrewed surface vehicles, that resemble small sailboats, in the North Atlantic Ocean in the vicinity of the Gulf Stream, we find that the estimate of the exchange of  $\text{CO}_2$  is larger when directly measured wind speeds are used in the calculation in comparison to wind speeds from a widely used data product. This result signifies the importance of co-located sensors on the same observing platform.

## 1. Introduction

The ocean absorbs approximately a quarter of all anthropogenic carbon dioxide ( $\text{CO}_2$ ) emissions each year, with uptake rates estimated at  $2.9 \pm 0.4 \text{ GtCyr}^{-1}$  in recent years (Friedlingstein et al., 2022). The uncertainty of the global ocean carbon uptake remains unacceptably high for verifying progress toward meeting climate policy agreements (Peters et al., 2017). The net uptake is the result of a small residual between ocean domains with strong ingassing, like the subtropical Western Boundary Currents, and strong outgassing, like the tropical Pacific upwelling region (Cronin et al., 2010). Uncertainty of regional fluxes is much higher relative to regional means than the global average (Fay & McKinley, 2021).

These uncertainties stem, in part, from sparse sampling. Currently, there are large swaths of the ocean that remain poorly sampled, with samples highly concentrated along specific shipping routes, and with a strong bias toward non-wintertime observations. These sampling biases in the present observational network lead to biases in the reconstructed surface ocean partial pressure of  $\text{CO}_2$  ( $p\text{CO}_2$ ) and air-sea  $\text{CO}_2$  flux (Hauck et al., 2023; Heimdal et al., 2023). Reducing these uncertainties motivates the need to substantially increase the number of observations, including through the use of novel observing platforms.

Many process studies rely on global data products to provide key variables needed in the calculation of air-sea CO<sub>2</sub> exchange. The goal of this research is to quantify the influence on bulk air-sea CO<sub>2</sub> fluxes when they are calculated using contemporaneous in situ observations, rather than a blend of these direct observations and data products, as is typical for regional and process studies. Constraining regional air-sea CO<sub>2</sub> fluxes will lead to better understanding of physical and biogeochemical processes that contribute to the global ocean sink (Fay & McKinley, 2021; McKinley et al., 2017).

### 1.1. Bulk Air-Sea CO<sub>2</sub> Exchange

Calculations of the air-sea flux of CO<sub>2</sub> depend on knowledge of *p*CO<sub>2</sub> in the lower atmosphere and surface ocean, wind speed, and—in some implementations of the empirical gas transfer velocity calculation—significant wave height. In many cases, one or more of these observations is lacking, due to the reliance on Ships of Opportunity, which are often cruise or cargo ships that are outfitted with limited meteorological and oceanographic instrumentation, or Research Vessels, which often only measure *p*CO<sub>2</sub> in the ocean but not the atmosphere due to challenges of removing the ship emissions from the data (Wanninkhof et al., 2019). Additionally, high-quality observations of *p*CO<sub>2</sub> are not standard on all Research Vessels and require a specific shipboard setup. Observations of all relevant variables in remote and extreme environments, like the Southern Ocean, are particularly scarce (Hauck et al., 2023; Landschützer et al., 2023). Therefore, it is important to evaluate the potential of novel platforms to provide observing capability in these regions, as well as understand the added value such platforms provide by measuring all variables needed for the calculation of air-sea CO<sub>2</sub> flux.

Bulk air-sea fluxes in ice-free regions for a slightly soluble gas, such as CO<sub>2</sub>, are estimated using the following formula (Fairall et al., 2003):

$$F = k\alpha\Delta pCO_2 \quad (1)$$

where *k* is the gas transfer velocity,  $\alpha$  is the solubility of CO<sub>2</sub> in seawater (dependent on sea surface temperature and salinity), and  $\Delta pCO_2$  is the air-sea difference of *p*CO<sub>2</sub> (ocean minus atmosphere). The gas transfer velocity, *k*, is typically expressed as a function of wind speed, such as in Ho et al. (2006) and Wanninkhof (2014) (W14 herein):

$$k = 0.251 U_{10}^2 \left( \frac{Sc}{660} \right)^{-1/2} \quad (2)$$

where *U*<sub>10</sub> is the wind speed at 10 m height and *Sc* is the Schmidt number.

Breaking waves and bubble injection contribute to air-sea CO<sub>2</sub> exchange in high wind conditions (Brumer et al., 2017; Edson et al., 2011; Woolf, 1997). Wind-only gas transfer velocity parameterizations, such as in Equation 2, do not explicitly account for the contribution of breaking waves and bubble injection to the air-sea CO<sub>2</sub> exchange and underestimate transfer under high wind speeds when compared to observations (Deike & Melville, 2018; Gu et al., 2021; Zhou et al., 2023). Some observational platforms provide data to calculate significant wave height, allowing for the implementation of a sea-state dependent gas transfer velocity equation. We expect the bubble contribution to the air-sea CO<sub>2</sub> flux to be especially important in the wintertime North Atlantic, which experiences strong, frequent storms that bring high wind speeds and large significant wave heights (Reichl & Deike, 2020; Zhou et al., 2023). One example of a sea-state dependent gas transfer velocity is that by Deike and Melville (2018) (DM18 herein):

$$k = \left[ A_{NB} u_* + \frac{A_B}{\alpha} \left( u_*^{5/3} \sqrt{gH_s}^{4/3} \right) \right] \cdot \left( \frac{Sc}{660} \right)^{-1/2} \quad (3)$$

where *A*<sub>NB</sub> and *A*<sub>B</sub> are empirical coefficients related to the non-bubble and bubble components of the gas transfer velocity, respectively. The friction velocity is *u*<sub>\*</sub> and can be represented as *u*<sub>\*</sub> =  $\sqrt{C_d} U_{10}$ , where *C*<sub>d</sub> is the drag coefficient. The non-dimensional solubility is  $\alpha$ , *g* is the gravitational constant, *Sc* is the Schmidt number, and *H*<sub>s</sub> is the significant wave height.

Among the many platforms collecting observations relevant for CO<sub>2</sub> exchange, surface moorings, uncrewed surface vehicles (USVs), and a small number research vessels stand out because they observe all the necessary variables contemporaneously. In contrast, the extensive Surface Ocean CO<sub>2</sub> Atlas (SOCAT) database contains millions of quality controlled observations dating back to 1957 (Bakker et al., 2016) but rarely includes co-located ocean  $p\text{CO}_2$ , atmospheric  $p\text{CO}_2$ , and wind speed data. Technologies like USVs provide an opportunity to evaluate the uncertainties arising from blending in situ observations and data products. They also can help fill large spatial and temporal gaps in the SOCAT Atlas, like in the wintertime and Southern Hemisphere (Sutton et al., 2021). Here we show the capability of one type of USV to sustain wintertime measurements in the challenging Gulf Stream region, a possible step toward instrumenting even more sparsely-observed regions in the ocean.

## 1.2. Saildrone USVs

Saildrone Explorer USVs have the ability to measure variables of the lower atmosphere and upper ocean which are necessary for calculating bulk air-sea fluxes (Gentemann et al., 2020; Nickford et al., 2022; Sutton et al., 2021; Zhang et al., 2019). For CO<sub>2</sub> fluxes, these variables include wind speed and direction, sea surface temperature, salinity, and atmospheric and surface ocean CO<sub>2</sub> mole fraction ( $\chi\text{CO}_2$ ). Significant wave height and dominant wave period can also be provided from the Saildrone's inertial measurement unit (IMU). The IMU consists of GPS, gyroscopes, accelerometers, and magnetometers which collectively allow for the calculation of platform acceleration and heave. From these motions, significant wave height and dominant wave period can be derived, according to the methods described by the National Data Buoy Center (Earle, 2003). The Saildrone vehicles are propelled by wind, and their batteries are charged with onboard solar panels and an underwater turbine. They travel at an average speed of 2–4 knots. Shore-based pilots send waypoints to the vehicles via iridium satellite communication and can make on the fly adjustments to their trajectories.

A recent study investigated the flow distortion of Saildrone in various wind-wave conditions and found that it is comparable to or less than that on ships and buoys (Reeves Eyre et al., 2023). Due to the position of the sonic anemometer at the forward edge of the Saildrone wing, it is thought that flow distortion is minimized (Gentemann et al., 2020). Wind speed observations between a Saildrone and a nearby ship compared well, with a root mean squared (RMS) difference of 0.62 m s<sup>-1</sup> and direction 3.8° (Cokelet et al., 2015). In the SPURS-2 campaign, compared to an ASIMET buoy, the RMS difference was 0.63 m s<sup>-1</sup> and 16° (Zhang et al., 2019). The difference between Saildrone and ASIMET buoys was attributed to flow distortion around the buoy. Gentemann et al. (2020) report that a National Data Buoy Center buoy had moderate bias of  $-0.32\text{ m s}^{-1}$  and direction 6.26° compared to Saildrone (for wind speeds  $>3\text{ m s}^{-1}$  to account for the high uncertainty in low wind speeds measured by the wind vane on the buoy). Ricciardulli et al. (2022) report that Saildrones have a  $-0.49\text{ m s}^{-1}$  bias compared to satellite wind products in the wind speed range 0–50 m s<sup>-1</sup>.

In this analysis, we compare the air-sea CO<sub>2</sub> flux calculated using contemporaneous, co-located measurements of wind speed, atmospheric mole fraction of CO<sub>2</sub> ( $\chi\text{CO}_2$ ; which is converted to  $p\text{CO}_2$ ), and significant wave height to the flux calculated when one or more of these variables are taken from a reanalysis or data-based product (generally referred to as “product” herein). Additionally, we assess the differences between using a wind-only (W14) and a sea-state dependent gas transfer velocity (DM18). To accomplish this research, we use in situ wintertime data collected in the Gulf Stream region of the North Atlantic. We focus our analysis on the wintertime (December through March) as this is the season when air-sea CO<sub>2</sub> fluxes are maximized due to strong wind events and low surface  $p\text{CO}_2$  in the cooled surface waters (Landschützer et al., 2013; Nickford et al., 2022; Takahashi et al., 2009). The paper is organized as follows: in Section 2 we describe the data collected during the observational missions, the data products we use, and outline the bulk air-sea CO<sub>2</sub> flux calculations for four different combinations of in situ and reanalysis data. In Section 3 we show the results of the intercomparison of Saildrone data with surface moorings and the ERA-5 reanalysis. In Section 4 we summarize our conclusions and provide recommendations based on our findings.

## 2. Methods

### 2.1. In Situ Observations

Observations collected during two Saildrone missions are used in this study: one from February 2019 (SD-1021) as described in Nickford et al. (2022), and a multi-Saildrone mission from December 2021–September 2022 (SD-1090, SD-1091, SD-1092, and SD-1089). For the 2021–2022 mission, we restrict the analysis through 31 March

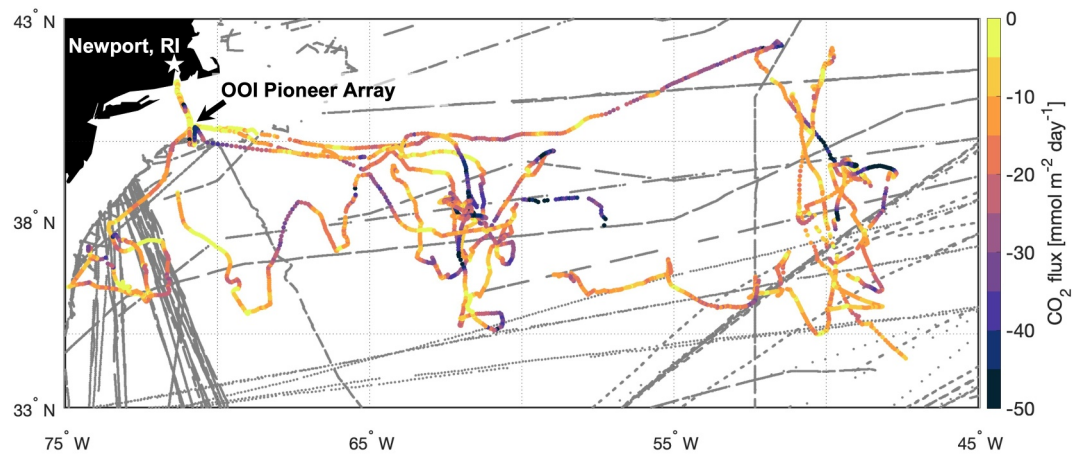


**Figure 1.** Bulk air-sea CO<sub>2</sub> fluxes calculated using Saildrone data in Equation 1 from the winters of 2019 and 2022 (colors). The gray tracks are the locations of historical wintertime (December–March) surface ocean  $p\text{CO}_2$  observations from 1957 to 2021 from the surface ocean CO<sub>2</sub> Atlas database excluding the continental shelf (water depth <200 m).

2022, when most of the observations were collected, and to focus on the wintertime. Between the two missions, we have 190 Saildrone-days of wintertime observations. The 2021–2022 observational campaign was designed to occupy crossings of the Gulf Stream at three different points along the current (Figure 1). Four Saildrones were used throughout the mission and were active for various period of times (Table 1).

Atmospheric and surface ocean CO<sub>2</sub> are measured by the ASVCO<sub>2</sub> Gen2 system, which has an air and seawater intake that pumps the sample through a bubble equilibrator before measuring the partially dried sample using a LI-COR 820 CO<sub>2</sub> Gas analyzer. Every sample measurement is preceded by two calibration points: a zero that is produced by drawing air through a soda lime column in a closed loop to scrub out all CO<sub>2</sub>, and a gas with a known CO<sub>2</sub> concentration, traceable to the World Meteorological Organization (Sabine et al., 2020; Sutton et al., 2014). The nominal measurement uncertainty of the ASVCO<sub>2</sub> is 2  $\mu\text{atm}$ , which is considered to be of “climate-quality” (Bender et al., 2002).

Saildrones SD-1090, SD-1091, and SD-1092 were launched from Newport, RI on 9–10 December 2021. They sailed southward together and circumnavigated the Ocean Observatories Initiative (OOI) Pioneer Array at the U. S. East Coast Shelfbreak for sensor intercomparison at a distance of 1–3 km (Figure 1; see Section 3.1 for results). SD-1090 then transited southwestward toward Cape Hatteras, NC to occupy the “upstream” location (74°W). SD-1091 transited eastward to the Tail of the Grand Banks, occupying the “downstream” location (50°W), while SD-1092 transited eastward to occupy the “mid-point” between the two near the New England Seamounts (61°W). Both the “midpoint” and “downstream” Gulf Stream regions have historically lacked  $p\text{CO}_2$  observations in wintertime: Over more than five decades of effort, each region had been sampled during only a handful of wintertime cruises (Figure 1).

**Table 1**  
*Saildrone Data Collection Range and Sensor Function for Each Platform*

Platform ID	Start	End	Dates of sensor issues (instrument/reasoning)
1021	30 January 2019	22 February 2019	22 February 2019 (platform damaged)
1090	9 December 2021	9 January 2022	4 January 2022 (platform damaged)
1091	9 December 2021	27 September 2022 <sup>a</sup>	24 January–13 February (all sensors turned off for battery conservation)
1092	10 December 2021	12 March 2022	14 December 2021 (SBE37 dissolved oxygen failure) 26 December 2021 (ASVCO <sub>2</sub> , valve malfunction) 12 March 2022 (platform damaged)
1089	11 February 2022	27 July 2022 <sup>a</sup>	5 March 2022 (SBE37 failure)

*Note.* The SBE37 measures conductivity, temperature, dissolved oxygen, and pressure. The ASVCO<sub>2</sub> measures ocean and atmosphere  $\chi\text{CO}_2$ . <sup>a</sup>Data collected beyond 31 Mar 2022 is omitted for this wintertime analysis.

With storms occurring weekly, the USVs experienced tropical storm strength winds ( $>17.5 \text{ m s}^{-1}$ ). SD-1090 was in a region where strong ocean surface current velocities opposed the wind direction as a powerful storm intensified, resulting in large, breaking waves that damaged the wing. The vehicle was subsequently routed back to land. SD-1092 also encountered damaging waves few months later on 12 March 2022 (Table 1). On 11 February 2022, SD-1089 was deployed to maintain the three drone occupation of the Gulf Stream. Upon launch, SD-1089 transited southward past the OOI Pioneer Array and met up with SD-1092 for intercomparison on 20 February. SD-1092 then transited toward the “upstream” position while SD-1089 transited east toward the “mid-point” location. The data from SD-1092 are omitted from the analysis during this period, 20–21 February 2022, because they were collected after its ASVCO<sub>2</sub> malfunctioned.

With skilled piloting, our Saildrone mission was able to circuit various positions in the Gulf Stream region and be brought in close proximity to one another, to surface moorings, and a Research Vessel for measurement intercomparisons. Several Saildrones withstood months of wintertime observations with damage occurring only under the most challenging sea state: surface ocean currents that oppose strong winds that quickly produce breaking waves taller than its 5 m rigid wing.

The SBE37 sensor on SD-1089 (installed at  $-1.9 \text{ m}$ ), which measures temperature, conductivity (used to calculate salinity), dissolved oxygen, and pressure, failed on 6 March 2022 (Table 1). A secondary temperature sensor, the RBR Coda3 (installed at  $-0.5 \text{ m}$ ), functioned properly throughout the mission. While both sensors were operating, the SST observations were consistently the same. The correlation coefficient between the two sensors is nearly 1 and the RMS error (RMSE) is  $0.05^\circ\text{C}$ . Therefore, we use the SST from the RBR Coda3, rather than from the SBE37 which is used for all other drones. To account for the missing salinity after the SBE37 failure, a temperature-salinity relationship is established by performing a linear regression during the period of time where the SBE37 was reliable (11 February 2022–5 March 2022):

$$S = 0.237 \cdot SST + 31.748 \quad (4)$$

where  $S$  is the salinity and  $SST$  is sea surface temperature. The equation is fit using the SBE37 observations and applied to the SST from the RBR Coda3. This estimated salinity is used throughout the SD-1089 analysis due to its close correspondence with measured salinity ( $r = 0.95, p < 0.05$  and RMSE = 0.45) during the period of time before the SBE37 failure (see Supporting Information S1). In this application, salinity is only needed in the calculation of the solubility of CO<sub>2</sub>. Uncertainties even as large as 1 PSU would have a negligible effect on the solubility and therefore the uncertainty introduced through this approximation should have a negligible effect on the air-sea CO<sub>2</sub> flux calculation.

## 2.2. Reanalysis and Data-Based Products

The ERA-5 reanalysis product from ECMWF is a model that assimilates observations to create a dynamically consistent reconstruction of atmospheric and ocean variables (Hersbach et al., 2020). The reanalysis product is available at 31 km spatial resolution and hourly temporal resolution. In our calculations of the gas transfer velocity, we use 10 m wind speeds and significant wave height from ERA-5, as explained in the following subsection. We also use the ERA-5 drag coefficient to calculate the friction velocity in the DM18 equation. Finally, we use surface pressure to convert atmospheric  $\chi\text{CO}_2$  to  $p\text{CO}_2$  (described below).

The NOAA Marine Boundary Layer (MBL) CO<sub>2</sub> zonal surface product provides lower atmosphere  $\chi\text{CO}_2$  at  $3^\circ$  latitude intervals each week (<https://gml.noaa.gov/cccg/mbl/mbl.html>). At the time of writing, this product is available from 1979 to 2022. We convert the estimated mole fractions to partial pressure using the surface pressure from the ERA-5 reanalysis (see Equation [5]), resulting in a  $p\text{CO}_2$  map at the spatial and temporal resolution of ERA-5.

## 2.3. Calculating the Air-Sea CO<sub>2</sub> Flux

Observations from each Saildrone platform are used during the period of time all necessary data are available (Table 1). The ASVCO<sub>2</sub> sensor measures the mole fraction of CO<sub>2</sub> and must be converted to partial pressure using the following equation:

$$pCO_2^{atm} = \chi CO_2^{atm} (P_{atm} - P_{H2O}) \quad (5)$$

where  $P_{atm}$  is the sea level pressure measured by the barometer on Saildrone and  $P_{H2O}$  is the saturation vapor pressure of water calculated using SST and salinity measured by Saildrone (Zeebe & Wolf-Gladrow, 2001).

We calculate fluxes according to four scenarios that correspond to the capabilities of current observational platforms and data pipelines:

- Scenario A—All observations in the bulk calculation are collected contemporaneously, as they are aboard Saildrone vehicles.
- Scenario B—Wind speed, ocean  $pCO_2$ , SST, and salinity from Saildrone are used. Atmospheric  $pCO_2$  is from the MBL product and significant wave height is from ERA-5. This scenario is typical of process studies using ocean  $pCO_2$  collected aboard a Research Vessel with wind speeds measured by the meteorological package onboard.
- Scenario C—Ocean  $pCO_2$ , atmospheric  $pCO_2$ , SST, salinity, and significant wave height from Saildrone are used. Wind speed is from ERA-5. This scenario could serve as guidance for when anemometers malfunction at sea.
- Scenario D—Ocean  $pCO_2$ , SST, and salinity from Saildrone are used. Atmospheric  $pCO_2$  is from the MBL product, wind speed and significant wave height are from ERA-5. This scenario is typical of process studies that use relevant data from the SOCAT database, which often lacks contemporaneous wind speed and atmospheric  $pCO_2$  observations.

For each scenario, the reanalysis or data-based product is linearly interpolated to the geographical position and time of the USV observations. The  $\Delta pCO_2$  is calculated by subtracting the atmospheric  $pCO_2$  (either directly observed from the Saildrone or estimated by the MBL product) from the ocean  $pCO_2$ . The solubility of  $CO_2$  in seawater is calculated using Saildrone SST and salinity observations in the formula from Weiss (1974) in all of the four scenarios. The Schmidt number, used in the gas transfer velocity calculations, is estimated using Saildrone SST observations (Wanninkhof, 2014).

The Coupled Ocean-Atmosphere Response Experiment (COARE) bulk algorithm for calculating air-sea fluxes is based on Monin-Obukhov Similarity Theory where the fluxes are represented in terms of mean variables that are more widely observed than fluxes themselves (Edson et al., 2013; Fairall et al., 2003). As an intermediate step, the COARE algorithm corrects input variables to a standard measurement height (typically 10 m). Saildrone wind speed, instantaneous anemometer height, air temperature, height of mounted air temperature sensor, relative humidity (RH), and height of mounted RH sensor, surface pressure, significant wave height and phase speed are input into COARE 3.5 algorithm for Matlab. We use the output U10 (wind corrected to the standard height of 10 m above the sea surface) which takes into account the platform tilt and atmospheric stability. The COARE 3.5 output of wind speed at 10 m height is smoothed using a 60-min moving average. We apply the same methodology for calculating the friction velocity in the DM18 formula.

### 3. Results and Discussion

#### 3.1. Intercomparison Among Saildrone and OOI Surface Moorings

We perform two types of intercomparisons to assess the quality of data collected by the USVs: Saildrone-Saildrone (Figure 2 and in Supporting Information S1) and Saildrone-mooring. For each, we compare the variables while the platforms were close to one another. The first period of intercomparison is when SD-1090, SD-1091, and SD-1092 were initially launched from Newport, RI and remained within 5 km of one another as they transited south toward the OOI Pioneer Array from December 10th through 13 December 2021. No height adjustments are made to the Saildrone observations for this comparison since all three platforms are outfitted with identical sensors. Upon launch, the  $pCO_2$  observations from SD-1091 are about 1  $\mu\text{atm}$  lower than that collected by SD-1090 and SD-1092. During another intercomparison period in April 2022, the  $pCO_2$  observations from SD-1091 are 3  $\mu\text{atm}$  lower in comparison to SD-1089 (not shown). This possible drift is close to the measurement uncertainty of the ASVCO<sub>2</sub> system (2  $\mu\text{atm}$ ; Sabine et al. (2020)). From 11–14 December 2021, all Saildrones recorded observations of wind speed, SST, salinity, dissolved oxygen, and atmospheric  $pCO_2$  that compared well with one another (Figure 2 and Supporting Information S1). At the end of the intercomparison period, on 13

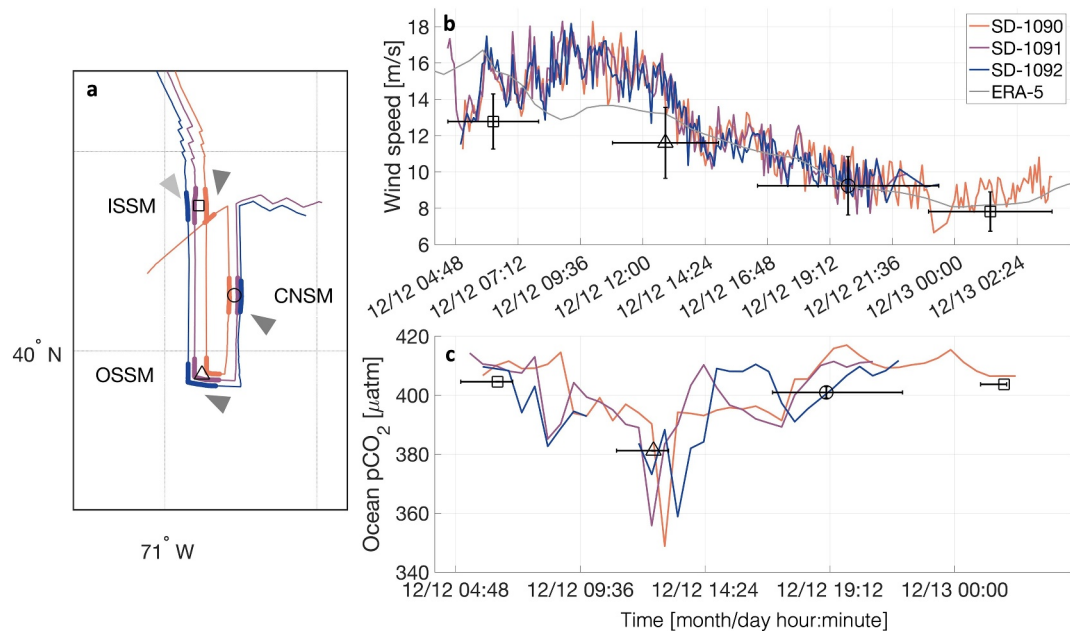


**Figure 2.** Intercomparison between Saildrone and OOI Pioneer Array. (a) Map showing the Pioneer Array buoys: inshore surface mooring (ISSM, black square), offshore surface mooring (OSSM, black triangle), and central surface mooring (CNSM, black circle). Saildrone paths are shown in colors with the bold segments indicating within 5 km of the mooring. Gray arrows indicate the direction that the wind is blowing during intercomparison time and the lighter gray arrow corresponds to the second intercomparison time between SD-1090 and ISSM. (b) Timeseries of U10 wind speed from each Saildrone compared to the average from the appropriate mooring when the Saildrones were within 10 km of the mooring. Moorings are indicated by marker shape as in panel (a). The vertical bars indicate standard deviation and horizontal bars indicate the intercomparison time period. Gray line is ERA-5 wind speed interpolated to the time and location of SD-1090. (c) same as in (b) but for ocean  $p\text{CO}_2$  within 5 km of each mooring.

December 2021, observations collected by SD-1090 differ from the other two Saildrones because it began to turn west while the others turned east.

As the Saildrones approached the OOI Pioneer Array, we compare atmospheric variables within 10 km from the surface moorings and ocean variables within 5 km (Figure 2a). We focus on the comparison of wind speed and ocean  $p\text{CO}_2$ , as these are the most relevant for calculating air-sea  $\text{CO}_2$  fluxes with a broader suite of intercomparisons listed in Tables 2 and 3. The Saildrones were between 1 and 3 km from each surface mooring at their closest approach. We note that this distance between the Saildrone and each surface mooring is large enough to eliminate the possibility of downstream flow distortion due to the presence of the Saildrones at the mooring site. OOI surface moorings (inshore surface mooring [ISSM], offshore surface mooring [OSSM], and central surface mooring [CNSM]) have an anemometer mounted at 3 m above the sea surface (the METBK package) but do not provide the instantaneous sensor height for each data point, which can change as the buoy leans under high winds and seas. Therefore we use the fixed 3 m height in COARE 3.5 (same for air temperature and RH) to estimate the U10 wind speeds to compare with Saildrone observations. Other variables are not height adjusted for comparison purposes due to close sensor installation height (surface moorings at 3 m and Saildrone at 2.3 m). The mean wind speed bias of ISSM relative to the Saildrones is  $<-2 \text{ m s}^{-1}$ , for OSSM it is  $<-3 \text{ m s}^{-1}$ , and for CNSM it is  $<-1.3 \text{ m s}^{-1}$  (Table 2; Figure 2b). To our knowledge, there are no published comparisons of wind speeds measured on Research Vessels relative to OOI surface moorings, as has been performed for the similar- but not identical- ASIMET buoys. The biases documented here are higher than those reported in the longer-duration comparisons between ship-based and ASIMET buoy measurements by Zhang et al. (2019) who note that flow distortion impacts surface mooring wind speed observations when compared to research vessels. They are also higher than the 5% bias estimated using a computational fluid dynamics approach for other surface moorings (Schlundt et al., 2020). We suspect flow distortion could be one cause of the OOI wind speed bias relative to Saildrone (see also, internal communication at OOI: [https://ooifb.org/wp-content/uploads/2018/May2018Meeting/Appendix\\_XI\\_OOI\\_Global\\_Array.pdf](https://ooifb.org/wp-content/uploads/2018/May2018Meeting/Appendix_XI_OOI_Global_Array.pdf)). At high wind speeds, the ERA-5 product estimates wind speeds that

**Table 2**

*Intercomparison of Atmospheric Variables When Individual Saildrones Were Within 10 km of Each OOI Surface Mooring*

ISSM	SD-1090	SD-1091	SD-1092
Wind speed (ms <sup>-1</sup> )	-1.28	-1.67	-1.82
Air temperature (°C)	0.02	0.24	0.23
Relative humidity (%)	-1.66	0.08	0.12
Barometric pressure (hPa)	-1.95	-2.53	-2.48
Atmospheric $pCO_2$ (μatm)	3.05	3.36	2.93
OSSM	SD-1090	SD-1091	SD-1092
Wind speed (ms <sup>-1</sup> )	-2.5	-2.41	-2.66
Air temperature (°C)	-0.11	-0.14	-0.15
Relative humidity (%)	0.93	0.29	0.09
Barometric pressure (hPa)	-2.47	-3.0	-2.68
Atmospheric $pCO_2$ (μatm)	1.62	2.71	2.37
CNSM	SD-1090	SD-1091	SD-1092
Wind speed (ms <sup>-1</sup> )	-1.23	-0.9	-1.23
Air temperature (°C)	-0.04	-0.03	-0.07
Relative humidity (%)	-0.97	-1.48	-0.95
Barometric pressure (hPa)	-2.26	-2.03	-2.78
Atmospheric $pCO_2$ (μatm)	-26.97	-24.97	-29.37

*Note.* Values are the mean bias for each mooring relative to each Saildrone.

are higher than the surface moorings but lower than the Saildrones; at low wind speeds, the Saildrones, surface moorings and ERA-5 show closer agreement (Figure 2b). This is an interesting result considering the wind speed observations from the surface moorings are assimilated into the ERA-5 reanalysis product.

Air temperature and RH generally compare well between measurements on each Saildrone and surface mooring. We find a bias of approximately 3 hPa in the barometric pressure (Table 2); however, this is a significant improvement following the results of Gentemann et al. (2020) which found a consistent bias in Saildrone observations of 13 hPa. The previously large bias was traced back to an instrument housing issue that has since been resolved.

We suspect the  $pCO_2$  sensor on CNSM malfunctioned during the intercomparison period; the atmospheric (ocean) observations are >20 μatm (7 μatm) lower than ISSM, OSSM, and all Saildrone vehicles (Tables 2 and 3), and the temporal variations recorded by CNSM do not match the other timeseries (not shown). In contrast, Saildrone atmosphere and ocean  $pCO_2$  observations compare well with ISSM and OSSM (Figure 2c and Table 3). The measurement uncertainty of the Pro-Oceanus  $pCO_2$ -pro instrument used on the surface moorings is estimated to be 6 μatm (Hartman et al., 2015). The low ocean  $pCO_2$  observations from CNSM could be attributed to a needed calibration of the OOI moorings; however, in situ bottle data from the deployment and recovery cruises are not yet available. It is possible that this is due to an instrument error but the behavior does not follow any of the detailed sensor issues described in Palevsky et al. (2022). The Saildrones observed an oceanic submesoscale event over a distance of 3.4 km on 12 December 2021, coinciding with the comparison with OSSM (Figure 2c). The feature had warm, salty, low oxygen waters and was associated with a 20 μatm ocean  $pCO_2$  drop (see Supporting Information S1).

At the mid-point of the 2022 Mission, a comparison of  $pCO_2$  between SD-1089 and bottle samples collected aboard the R/V Endeavor was conducted. The SD-1089  $pCO_2$  was compared to a surface bucket sample and surface CTD cast. The  $pCO_2$  from the bucket sample and CTD cast is estimated using dissolved inorganic carbon (DIC), total alkalinity (TA) and pH discrete samples in the carbonate system solver called CO2SYS (Lewis & Wallace, 1998). The surface samples and SD-1089 ocean  $pCO_2$  observations agree within measurement uncertainty of  $\pm 8.3$  μatm. Therefore, we do not suspect that the ASVCO<sub>2</sub> drifted substantially over time on SD-1089.

### 3.2. Saildrone Observes Wind Speeds Higher Than ERA-5

Figure 3 compares all of the wind speeds measured on the Saildrone vehicles and corrected to a 10 m standard height to the ERA-5 winds interpolated to the Saildrone location and time (RMSE = 1 m s<sup>-1</sup> and mean bias = -0.27 m s<sup>-1</sup>). The ERA-5 product captures essentially all of the rapid variability in wintertime winds at each of the Saildrone positions along the Gulf Stream. Nevertheless, Figure 3 hints at a bias in ERA-5 winds during the highest wind speed events.

Figure 4a gives a more quantitative view of how the ERA-5 product underestimates the wind speed compared to the Saildrone observations at all wind speeds greater than 10 m s<sup>-1</sup>. About half of the hourly averaged observations collected during the mission are during high wind speed conditions (>10 m s<sup>-1</sup>) when Saildrone-ERA-5 differences are more substantial, as shown in Figure 4a where the ERA-5 bin averages fall below the 1:1 line.

**Table 3**

*Intercomparison of Ocean Variables When Individual Saildrones Were Within 5 km of Each OOI Surface Mooring*

ISSM	SD-1090	SD-1091	SD-1092
SST (°C)	-0.06	0.04	-0.02
Salinity	0.02	0.01	-0.01
Ocean $pCO_2$ (μatm)	-4.19	-5.4	-3.62
OSSM	SD-1090	SD-1091	SD-1092
SST (°C)	0.01	-0.07	-0.31
Salinity	0.02	-0.02	-0.17
Ocean $pCO_2$ (μatm)	-1.4	4.19	0.78
CNSM	SD-1090	SD-1091	SD-1092
SST (°C)	-0.0009	-0.01	-0.04
Salinity	0.03	0.01	-0.01
Ocean $pCO_2$ (μatm)	-7.85	-7.98	-9.0
Significant wave height (m)	-0.14	-0.1	-0.05
Dominant wave period (s)	-1.71	-0.33	1.16

*Note.* Values are the mean bias for each mooring relative to each Saildrone.

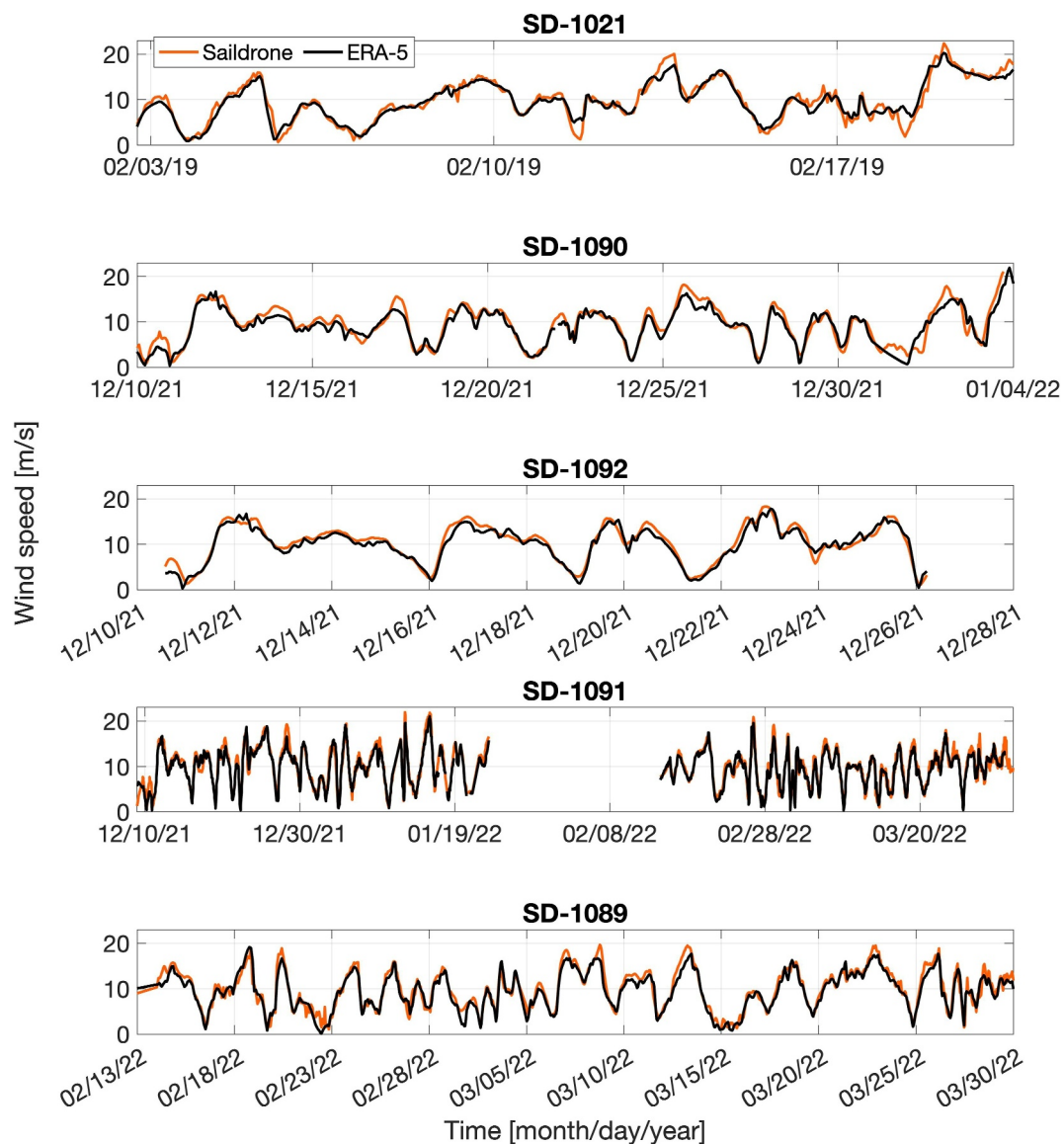


**Figure 3.** Saildrone wind speed (U10) comparison with ERA-5. Each panel is the hourly average wind speed timeseries from each Saildrone corrected to 10 m standard height using COARE3.5 (orange lines). The ERA-5 10 m wind speed is interpolated to the time and location of each Saildrone (black lines). Note that the time on the x-axis is not consistent for each Saildrone due to different deployment periods.

Other studies have found that ERA-5 tends to underestimate wind speeds: for instance, Kalverla et al. (2020) find an underestimate of ERA-5 wind speeds by  $0.5 \text{ m s}^{-1}$  relative to a wind observation tower in the North Sea. Susini et al. (2022) show that ERA-5 underestimates wind speeds  $>10 \text{ m s}^{-1}$  compared to observations from data stations on wind turbines in the North Sea. An ERA-5 wind speed bias of  $-2 \text{ m s}^{-1}$  ( $\text{RMSE} > 3 \text{ m s}^{-1}$ ) compared to satellite observations, particularly in mid latitude western boundary current regions, was also noted by Campos et al. (2022). ERA-5 underestimates the highest wind speeds that occur during winter storm events, as stated by Belmonte Rivas and Stoffelen (2019) who showed that ERA-5 underestimates surface transient winds (storms) particularly in midlatitudes when compared to satellite winds.

The ERA-5 wind speed bias is important because the highest probability for wind speed observations is within the  $10\text{--}12 \text{ m s}^{-1}$  range during our wintertime Gulf Stream survey (Figure 4a). Like the comparison of wind speeds, the ERA-5 estimate of friction velocity is also lower than the Saildrone estimates in the high wind speed range (Figure 4b). The probability of friction velocity observations is highest in the  $0.1\text{--}0.5$  range which are typical

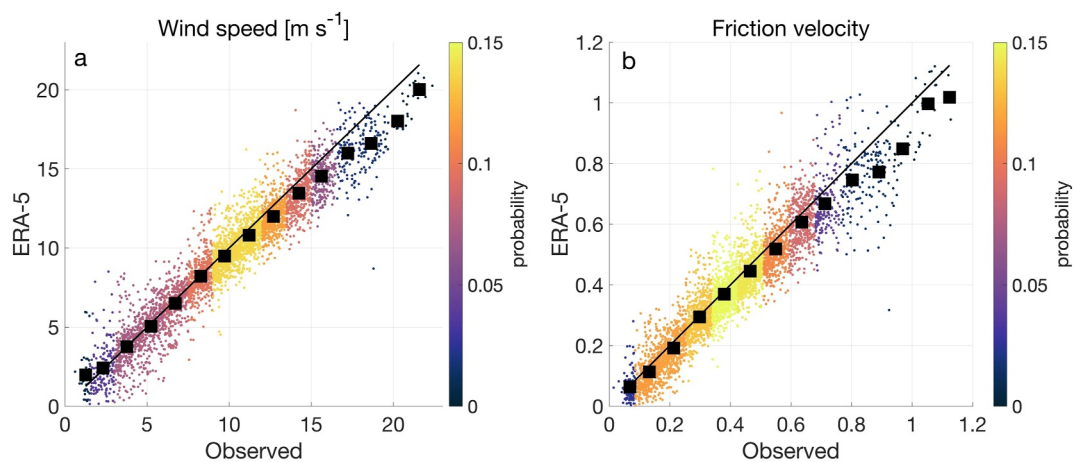


**Figure 4.** (a) ERA-5 wind speed and (b) friction velocity interpolated to the hourly Saildrone time and position versus directly measured wind speed (adjusted to 10 m) and the friction velocity from COARE3.5. The probability of (a) wind speed and (b) friction velocity to fall into defined bins with increments 1.5 m/s or 0.085, respectively, are shaded in colors. Black squares represent the average value of ERA-5 estimates versus the average value of observations within each bin. The 1:1 line is shown in solid black.

values over the ocean (and correspond to wind speeds in the 5–15 m s<sup>-1</sup> range). Despite the remarkable overall agreement of ERA-5 with in situ observations shown in Figure 3, the systematic underestimate of the highest wind speed events has a significant impact on the calculation of the air-sea CO<sub>2</sub> flux, as discussed in Section 3.4.

### 3.3. Sea-State Dependent Gas Transfer Velocity Yields Larger Ocean CO<sub>2</sub> Uptake

The sea-state dependent gas transfer velocity explicitly accounts for breaking waves and bubbles that mediate gas exchange. Figure 5 shows the air-sea CO<sub>2</sub> flux for Scenario A using the DM18 gas transfer velocity versus the flux calculated using the W14 equation. Generally, at low and moderate wind speeds, the W14 equation estimates

slightly greater ocean CO<sub>2</sub> uptake compared to DM18. At high wind speeds, the uptake estimated by DM18 is much greater than what is expected when using W14. This is likely due to the bubble term dominating at wind speeds  $>15$  m s<sup>-1</sup>, as stated by Deike and Melville (2018). The air-sea fluxes calculated using DM18 result in a 28% larger ocean uptake of CO<sub>2</sub> compared to that calculated using the wind-only gas transfer velocity from W14 (Figure 5; Table 4). This difference is substantial, likely due to the strong winds producing breaking waves in the North Atlantic, paired with large air-sea CO<sub>2</sub> gradients which enhance this exchange. This highlights the importance of gas transfer velocity equation selection in regional studies where frequent storms occur.

This result shows that the selection of gas transfer velocity equations is important to the resulting CO<sub>2</sub> flux. We chose to use the sea-state dependent equation in this work because of the known storminess of the North Atlantic. Using a sea-state dependent gas transfer velocity would likely enhance air-sea exchange in other ocean regions that experience frequent strong winds and breaking waves.

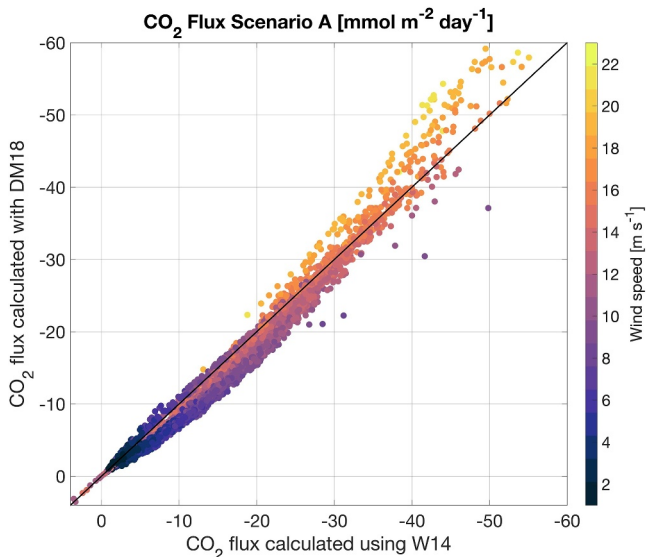


**Figure 5.** Air-sea CO<sub>2</sub> flux for Scenario A using the DM18 gas transfer velocity versus the W14 gas transfer velocity, colored by the observed wind speed. The 1:1 line is shown in solid black. Note that the axes are flipped because a majority of the CO<sub>2</sub> flux is negative, indicating ocean uptake. Points above the 1:1 line indicate that fluxes calculated with DM18 suggest more ocean carbon uptake while points below the line indicate that W14's wind-only relationship results in more ocean carbon uptake.

### 3.4. Co-Located Observations Increase Air-Sea CO<sub>2</sub> Flux Estimates by 9%

Figure 6 compares each scenario to Scenario A, in which all observations are collected contemporaneously on the same platform. Substituting the MBL CO<sub>2</sub> product and ERA-5 significant wave height in place of the in situ observations results in a 2% difference in the CO<sub>2</sub> flux (Figure 6a; Table 4).

**Table 4**Average Air-Sea  $\text{CO}_2$  Fluxes for Each Scenario ( $\text{mmol m}^{-2} \text{ day}^{-1}$ )

Air-sea $\text{CO}_2$ flux ( $\text{mmol m}^{-2} \text{ day}^{-1}$ )	Observed $\text{CO}_2^{\text{atm}}$ Observed $\text{H}_s$	MBL $\text{CO}_2^{\text{atm}}$ ERA-5 $\text{H}_s$
Observed wind speed	Scenario A	Scenario B
<b>DM18</b>	<b>-14.3</b>	<b>-14.0</b>
W14	-11.1	-11.0
ERA-5 wind speed	Scenario C	Scenario D
<b>DM18</b>	<b>-13.2</b>	<b>-13.0</b>
W14	-10.3	-10.1

*Note.* The top bold number is the flux calculated using DM18 gas transfer velocity and the bottom number is that using the W14 gas transfer velocity. The different scenarios correspond to those described in Section 2.3.

Compared to contemporaneous observations (Scenario A), substituting the ERA-5 wind speed product in the  $\text{CO}_2$  flux calculation (Scenario C) can cause up to an 8% reduction in ocean  $\text{CO}_2$  uptake (Table 4 and Figure 6b). These differences in air-sea  $\text{CO}_2$  flux mainly occur at the highest wind speeds due to the ERA-5 low bias as described in Section 3.2. Using all products in place of contemporaneous in situ wind speed, atmospheric  $\text{CO}_2$ , and significant wave height (Scenario D) lead to a 9% reduction compared to the contemporaneous observations (Figure 6c; Table 4). This difference is consistent for both gas transfer velocities.

We performed additional tests (not shown) to separate the relative influence of substituting the MBL atmospheric  $\text{CO}_2$  product in place of the in situ atmospheric  $\text{CO}_2$  measured by the Saildrone; this accounts for a 1% difference in the air-sea  $\text{CO}_2$  flux. We also found that only substituting the ERA-5 product for significant wave height accounts for 1% difference compared to using that calculated from Saildrone observations (also not shown). This analysis reveals that it is important to observe  $p\text{CO}_2$  in the ocean and atmosphere and wind speed contemporaneously to minimize bias in the air-sea  $\text{CO}_2$  flux.

#### 4. Conclusions

In this work, we explored the precision of the Saildrone observations needed for the calculation of air-sea  $\text{CO}_2$  exchange. First, we compared data collected by sensors across three platforms sailing for several days within a few kilometers of one another. This comparison showed a high level of consistency from measurements on the relevant sensors across the three platforms (Figure 2, Figures S2–S6 in Supporting Information S1). In addition, a comparison of the Saildrone data to OOI Pioneer surface moorings revealed strong agreement among all three Saildrones and mooring measurements of ocean  $p\text{CO}_2$ , SST and surface salinity measurements (Table 3), as well as surface air temperature and relative humidity (Table 2). The Saildrone USVs recorded about 2–3 hPa higher barometric pressure than the moorings, a substantially reduced bias since changes to the pressure instrument housing on the Saildrones were made (Gentemann et al., 2020). The atmospheric and ocean  $p\text{CO}_2$  measured by all Saildrones corresponds well with the OOI measurements aboard two moorings (ISSM and OSSM; see Tables 2 and 3), while CNSM  $p\text{CO}_2$  differed substantially from all other platforms in both the ocean and atmosphere and, therefore, assumed the sensor on CNSM is assumed to be in error. The wind speeds measured aboard the OOI surface moorings were systematically lower than both the Saildrone wind speeds and the ERA-5 reanalysis wind speeds interpolated to the same position; such “underspeeding” by OOI anemometers is a known issue under investigation by OOI principal investigators (personal communication, Al Plueddemann 09/20/2023).

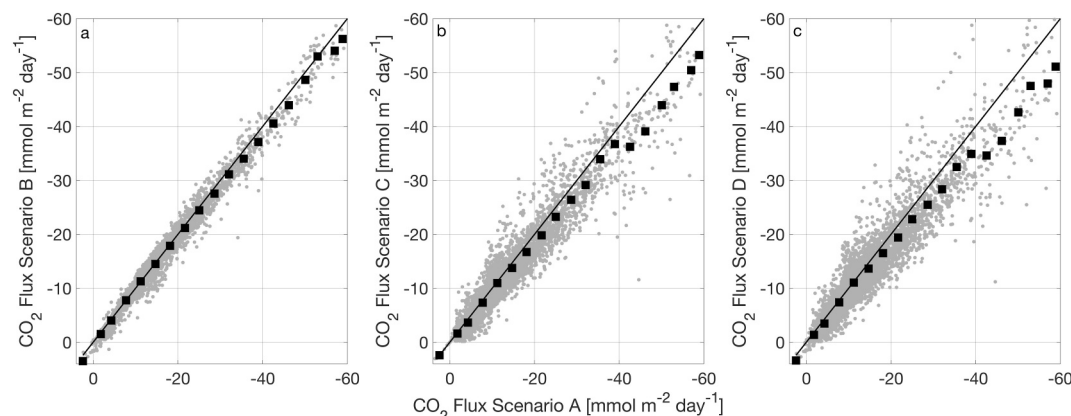


**Figure 6.** Air-sea  $\text{CO}_2$  flux estimates for Scenario A using the DM18 gas transfer velocity compared to Scenario B (a), Scenario C (b), and Scenario D (c). The black squares represent bin sizes of  $3.5 \text{ mmol m}^{-2} \text{ day}^{-1}$ . The 1:1 line is shown in solid black. Note that the axes are flipped because a majority of the  $\text{CO}_2$  flux is negative, indicating ocean uptake. Points above the 1:1 line indicate that the scenario on the y-axis suggests more ocean carbon uptake while points below the line indicate that Scenario A results in more ocean carbon uptake.

Following these intercomparisons, we used the Saildrone data to explore the value of simultaneously measuring all variables needed to calculate air-sea CO<sub>2</sub> fluxes via bulk formulas relative to the common situation where one or more variables is missing, and therefore inferred from relatively coarse-resolution, publicly available, data-based products. The Saildrone data were collected in the wintertime in the Gulf Stream region, where strong winds and large air-sea *p*CO<sub>2</sub> gradients are common, thus maximizing ocean carbon uptake. The ERA-5 reanalysis winds contain much of the variability in the winds as measured aboard the Saildrone vehicles (Figure 3). However, the ERA-5 product tends to be biased low when wind speeds exceed 10 m s<sup>-1</sup> (Figure 4). This systematic bias in wind speed translates to an 8% underestimate in the air-sea CO<sub>2</sub> flux when using the ERA-5 product in place of in situ wind speeds. The low bias increases to 9% when wind speed and significant wave height from ERA-5 and the MBL zonal mean atmospheric *p*CO<sub>2</sub> product are used in place of in situ data, signaling that the true atmospheric *p*CO<sub>2</sub> is higher than its zonal mean in this region downwind of North America (Palter et al., 2023). These biases are similar as a percentage error whether using a wind-only gas transfer velocity (e.g., Ho et al., 2006; Wanninkhof, 2014) or one that uses significant wave height to parameterize the bubble-mediated flux (Deike & Melville, 2018), while the difference in average flux between these two gas transfer velocities is over 25%.

Although ERA-5 and NOAA's MBL product provide reasonable estimates of wind speed and atmospheric *p*CO<sub>2</sub>, this work has shown that contemporaneous measurements of wind, ocean *p*CO<sub>2</sub>, and atmospheric *p*CO<sub>2</sub> are needed to avoid introducing a low bias of up to 9% in the calculation of air-sea CO<sub>2</sub> exchange in the Gulf Stream region. Though this bias pertains to a particular region and time of year, an open question for future research is: how might this underestimation of ocean carbon uptake impact the broader regional and global estimates?

Saildrone USVs showed considerable promise in delivering data at the air-sea interface for several months in one of the most extreme ocean environments on Earth. While breaking waves that crest over the Saildrone 5 m rigid wing can damage the platforms, these conditions are relatively rare in some regions and were often successfully avoided by active piloting during our mission. With this strategy, we sustained full winter observations by 2 Saildrones in the punishing Gulf Stream region. Moving forward to a more certain quantification of regional ocean carbon uptake would benefit from a strategy that incorporates sustained, comprehensive observations at the air-sea interface (Cronin et al., 2023).

## Data Availability Statement

Barometric pressure, wind speed, and significant wave height data from the ERA-5 reanalysis (Hersbach et al., 2023). The atmospheric  $\chi$  CO<sub>2</sub> is from the NOAA Marine Boundary Layer zonal mean CO<sub>2</sub> product (Lan et al., 2023). For the intercomparison with the OOI Pioneer Northeast Shelf Array, we used variables collected by the Bulk Meteorology Instrument Package, Air-Sea Interface *p*CO<sub>2</sub>, and Surface Wave Spectra instruments from the CNSM, OSSM, and ISSM surface buoys which are available at <https://dataexplorer.oceanobservatories.org> (NSF Ocean Observatories Initiative, 2023). Saildrone data from the 2019 (Palter et al., 2020) and 2021–2022 missions (Palter & Nickford, 2023) are publicly available. The software used for data processing and visualization is MATLAB R2021b (2021) with access through the University of Rhode Island license 40824201. The Matlab version of the COARE 3.5 algorithm is available at <https://github.com/NOAA-PSL/COARE-algorithm/tree/5b144cf6376a98b42200196d57ae40d791494abe/Matlab/COARE3.5> (COARE3.5 algorithm, 2013). The Air-sea CO<sub>2</sub> flux calculations in Matlab are available on GitHub [https://github.com/snicketford/Airsea\\_fluxes\\_Matlab.git](https://github.com/snicketford/Airsea_fluxes_Matlab.git) (Air Sea Fluxes Matlab, 2023). The color maps were provided by emoceane (Thyng et al., 2016).

## Acknowledgments

We gratefully acknowledge the reviewers for providing thoughtful feedback which contributed to improvements in this manuscript. Funding for data collected and used in this work was granted by Google.org Impact Challenge on Climate, the Saildrone Award, and the Rhode Island Endeavor Program. Student support was obtained by URI Dean's Fellowship. This work was also supported by NSF 2148276. We would like to acknowledge Dr. Hongjie Wang and Fiona Teevan-Kamhawai for analyzing the in situ bottle samples from the R/V Endeavor cruise. We would also like to thank the crew and science party aboard the R/V Endeavor.

## References

- Air Sea Fluxes Matlab. (2023). GitHub [Software] Retrieved from [https://github.com/snicketford/Airsea\\_fluxes\\_Matlab](https://github.com/snicketford/Airsea_fluxes_Matlab)
- Bakker, D. C., Pfeil, B., Landa, C. S., Metzl, N., O'Brien, K. M., Olsen, A., et al. (2016). A multi-decade record of high-quality *f*CO<sub>2</sub> data in version 3 of the Surface Ocean CO<sub>2</sub> Atlas (SOCAT). *Earth System Science Data*, 8(2), 383–413. <https://doi.org/10.5194/essd-8-383-2016>
- Belmonte Rivas, M., & Stoffelen, A. (2019). Characterizing ERA-Interim and ERA5 surface wind biases using ASCAT. *Ocean Science*, 15(3), 831–852. <https://doi.org/10.5194/os-15-831-2019>
- Bender, M., Doney, S., Feely, R., Fung, I., Gruber, N., Harrison, D., et al. (2002). A large-scale CO<sub>2</sub> observing plan: In situ oceans and atmosphere (LSCOP). *In Situ large-scale CO<sub>2</sub> observations working group*.
- Brumer, S. E., Zappa, C. J., Blomquist, B. W., Fairall, C. W., Cifuentes-Lorenzen, A., Edson, J. B., et al. (2017). Wave-related Reynolds number parameterizations of CO<sub>2</sub> and DMS transfer velocities. *Geophysical Research Letters*, 44(19), 9865–9875. <https://doi.org/10.1002/2017GL074979>
- Campos, R. M., Gramcianinov, C. B., De Camargo, R., & Da Silva Dias, P. L. (2022). Assessment and calibration of ERA5 severe winds in the Atlantic Ocean using satellite data. *Remote Sensing*, 14(19), 4918. <https://doi.org/10.3390/rs14194918>

COARE3.5 algorithm. (2013). GitHub [Software]. Retrieved from <https://github.com/NOAA-PSL/COARE-algorithm/tree/5b144cf6376a98b42200196d57ae40d791494abe/Matlab/COARE3.5>

Cokelet, E. D., Meinig, C., Lawrence-Slavas, N., Stabeno, P. J., Mordy, C. W., Tabisola, H. M., et al. (2015). The use of Saildrones to examine spring conditions in the Bering Sea. In *Oceans 2015 - MTS/IEEE Washington* (pp. 1–7). IEEE. Retrieved from <https://doi.org/10.23919/OCEANS.2015.7404357>

Cronin, M. F., Bond, N., Booth, J., Ichikawa, H., Joyce, T. M., Kubota, M., et al. (2010). Monitoring Ocean-atmosphere interactions in western boundary current extensions. *Proceedings of OceanObs'09: Sustained Ocean Observations and Information for Society*, 9. <https://doi.org/10.5270/oceanobs09.cwp.20>

Cronin, M. F., Swart, S., Marandino, C. A., Anderson, C., Browne, P., Chen, S., et al. (2023). Developing an observing air-sea interactions strategy (OASIS) for the global ocean. *ICES Journal of Marine Science*, 80(2), 367–373. <https://doi.org/10.1093/icesjms/fsac149>

Deike, L., & Melville, W. K. (2018). Gas transfer by breaking waves. *Geophysical Research Letters*, 45(19), 10482–10492. <https://doi.org/10.1029/2018GL078758>

Earle, M. D. (2003). Nondirectional and directional wave data analysis procedures. Retrieved from <https://www.ndbc.noaa.gov/wavemeas.pdf>

Edson, J. B., Fairall, C. W., Bariteau, L., Zappa, C. J., Cifuentes-Lorenzen, A., McGillis, W. R., et al. (2011). Direct covariance measurement of CO<sub>2</sub> gas transfer velocity during the 2008 Southern Ocean Gas Exchange Experiment: Wind speed dependency. *Journal of Geophysical Research*, 116(11), 1–24. <https://doi.org/10.1029/2011JC007022>

Edson, J. B., Jampana, V., Weller, R. A., Bigorre, S. P., Plueddemann, A. J., Fairall, C. W., et al. (2013). On the exchange of momentum over the open ocean. *Journal of Physical Oceanography*, 43(8), 1589–1610. <https://doi.org/10.1175/JPO-D-12-0173.1>

Fairall, C. W., Bradley, E. F., Hare, J. E., Grachev, A. A., & Edson, J. B. (2003). Bulk parameterization of air-sea fluxes: Updates and verification for the COARE algorithm. *Journal of Climate*, 16(4), 571–591. [https://doi.org/10.1175/1520-0442\(2003\)016<0571:bpofas>2.0.co;2](https://doi.org/10.1175/1520-0442(2003)016<0571:bpofas>2.0.co;2)

Fay, A. R., & McKinley, G. A. (2021). Observed regional fluxes to constrain modeled estimates of the ocean carbon sink. *Geophysical Research Letters*, 48(20), 1–11. <https://doi.org/10.1029/2021GL095325>

Friedlingstein, P., O'Sullivan, M., Jones, M. W., Andrew, R. M., Gregor, L., Hauck, J., et al. (2022). Global carbon budget 2022. *Earth System Science Data*, 14(11), 4811–4900. <https://doi.org/10.5194/essd-14-4811-2022>

Gentemann, C. L., Scott, J. P., Mazzini, P. L. F., Pianca, C., Akella, S., Minnett, P. J., et al. (2020). Saildrone: Adaptively sampling the marine environment. *Bulletin of the American Meteorological Society*, 101(6), E744–E762. <https://doi.org/10.1175/BAMS-D-19-0015.1>

Gu, Y., Katul, G. G., & Cassar, N. (2021). The intensifying role of high wind speeds on air-sea carbon dioxide exchange. *Geophysical Research Letters*, 48(5), 1–10. <https://doi.org/10.1029/2020GL090713>

Hartman, S. E., Jiang, Z.-P., Turk, D., Lampitt, R. S., Frigstad, H., Ostle, C., & Schuster, U. (2015). Biogeochemical variations at the porcupine abyssal plain sustained observatory in the northeast Atlantic Ocean, from weekly to inter-annual timescales. *Biogeosciences*, 12(3), 845–853. <https://doi.org/10.5194/bg-12-845-2015>

Hauck, J., Nissen, C., Landschützer, P., Rödenbeck, C., Bushinsky, S., & Olsen, A. (2023). Sparse observations induce large biases in estimates of the global ocean CO<sub>2</sub> sink: An ocean model subsampling experiment. *Philosophical Transactions of the Royal Society A: Mathematical, Physical & Engineering Sciences*, 381(2249), 20220063. <https://doi.org/10.1098/rsta.2022.0063>

Heimdal, T. H., McKinley, G. A., Sutton, A. J., Fay, A. R., & Goege, L. (2023). Assessing improvements in global ocean pCO<sub>2</sub> machine learning reconstructions with Southern Ocean autonomous sampling (preprint). *Biogeochemistry: Greenhouse Gases*. <https://doi.org/10.5194/bg-2023-160>

Hersbach, H., Bell, B., Berrisford, P., Biavati, G., Horányi, A., Muñoz Sabater, J., et al. (2023). ERA5 hourly data on single levels from 1940 to present [Dataset]. *Copernicus Climate Change Service (C3S) Climate Data Store (CDS)*. <https://doi.org/10.24381/cds.adbb2d47>

Hersbach, H., Bell, B., Berrisford, P., Hirahara, S., Horányi, A., Muñoz-Sabater, J., et al. (2020). The ERA5 global reanalysis. *Quarterly Journal of the Royal Meteorological Society*, 146(730), 1999–2049. <https://doi.org/10.1002/qj.3803>

Ho, D. T., Law, C. S., Smith, M. J., Schlosser, P., Harvey, M., & Hill, P. (2006). Measurements of air-sea gas exchange at high wind speeds in the Southern Ocean: Implications for global parameterizations. *Geophysical Research Letters*, 33(16), 1–6. <https://doi.org/10.1029/2006GL026817>

Kalverla, P. C., Holtslag, A. A. M., Ronda, R. J., & Steeneveld, G. (2020). Quality of wind characteristics in recent wind atlases over the North Sea. *Quarterly Journal of the Royal Meteorological Society*, 146(728), 1498–1515. <https://doi.org/10.1002/qj.3748>

Lan, X., Tans, P., Thoning, K., & NOAA Global Monitoring Laboratory. (2023). NOAA greenhouse gas marine boundary layer reference - CO<sub>2</sub> [Dataset]. *Global Monitoring Laboratory*. <https://doi.org/10.15138/DVNP-F961>

Landschützer, P., Gruber, N., Payne, M. R., Schuster, U., Bakker, D. C. E., Nakao, S., et al. (2013). A neural network-based estimate of the seasonal to inter-annual variability of the Atlantic Ocean carbon sink. *Biogeosciences*, 10(11), 7793–7815. <https://doi.org/10.5194/bg-10-7793-2013>

Landschützer, P., Tanhua, T., Behncke, J., & Keppler, L. (2023). Sailing through the southern seas of air-sea CO<sub>2</sub> flux uncertainty. *Philosophical Transactions of the Royal Society A: Mathematical, Physical & Engineering Sciences*, 381(2249), 20220064. <https://doi.org/10.1098/rsta.2022.0064>

Lewis, E., & Wallace, D. (1998). Program developed for CO<sub>2</sub> system calculations. Retrieved from <http://cdiac.esd.ornl.gov/oceans/co2prtnbk.html>

McKinley, G. A., Fay, A. R., Lovenduski, N. S., & Pilcher, D. J. (2017). Natural variability and anthropogenic trends in the ocean carbon sink. *Annual Review of Marine Science*, 9(1), 125–150. <https://doi.org/10.1146/annurev-marine-010816-060529>

Nickford, S., Palter, J. B., Donohue, K., Fassbender, A. J., Gray, A. R., Long, J., et al. (2022). Autonomous wintertime observations of air-sea exchange in the Gulf Stream reveal a perfect storm for ocean CO<sub>2</sub> uptake. *Geophysical Research Letters*, 49(5), e2021GL096805. <https://doi.org/10.1029/2021GL096805>

NSF Ocean Observatories Initiative. (2023). Bulk Meteorology instrument package (METBK), Air-Sea Interface pCO<sub>2</sub> (PCO2A), and surface wave Spectra (WAVSS) (CP04OSSM-SBD11-06-METBKA000, CP04OSSM-SBD12-04-PCO2AA000, CP03ISSM-SBD11-06-METBKA000, CP03ISSM-SBD12-04-PCO2AA000, CP01CNSM-SBD11-06-METBKA000, CP01CNSM-SBD12-04-PCO2AA000, CP01CNSM-SBD12-05-WAVSSA000) data from Pioneer NES Array from 2021-11-22 to 2021-12-19 [Dataset]. *Data Explorer ERDDAP*. Retrieved from <https://erddap.dataexplorer.oceanobservatories.org>

Palevsky, H., Clayton, S., Atamanchuk, D., Battisti, R., Batryn, J., Bourbonnais, A., et al. (2022). OOI biogeochemical sensor data best practices and user guide. Version 1.0.0. Retrieved from <https://repository.oceanbestpractices.org/handle/11329/2112>

Palter, J., & Nickford, S. (2023). The winter subset of the Saildrone 2021–2022 Mission to the Gulf Stream used for the publication the importance of contemporaneous measurements for regional air-sea CO<sub>2</sub> flux estimates [Dataset]. Zenodo. <https://doi.org/10.5281/ZENODO.8356237>

Palter, J., Nickford, S., & Mu, L. (2023). Ocean carbon dioxide uptake in the tailpipe of industrialized continents. *Geophysical Research Letters*, 50(21), e2023GL104822. <https://doi.org/10.1029/2023GL104822>

Palter, J., Nickford, S., Sutton, A. J., Gray, A. R., Fassbender, A. J., Maenner Jones, S., et al. (2020). Surface underway measurements of partial pressure of carbon dioxide ( $p\text{CO}_2$ ), sea surface temperature, sea surface salinity and other parameters from Autonomous Surface Vehicle ASV\_saildrone1021\_gulfstream (EXPOCODE 32DB20190130) in the North Atlantic Ocean from 2019-01-30 to 2019-02-21 (NCEI Accession 0209698) [Dataset]. NASA <https://doi.org/10.25921/2DW3-D527>

Peters, G. P., Le Quéré, C., Andrew, R. M., Canadell, J. G., Friedlingstein, P., Ilyina, T., et al. (2017). Towards real-time verification of  $\text{CO}_2$  emissions. *Nature Climate Change*, 7(12), 848–850. <https://doi.org/10.1038/s41558-017-0013-9>

Reeves Eyre, J. E. J., Cronin, M. F., Zhang, D., Thompson, E. J., Fairall, C. W., & Edson, J. B. (2023). Saildrone direct covariance wind stress in various wind and current regimes of the tropical Pacific. *Journal of Atmospheric and Oceanic Technology*, 40(4), 503–517. <https://doi.org/10.1175/JTECH-D-22-0077.1>

Reichl, B. G., & Deike, L. (2020). Contribution of sea-state dependent bubbles to Air-Sea carbon dioxide fluxes. *Geophysical Research Letters*, 47(9), e2020GL087267. <https://doi.org/10.1029/2020GL087267>

Ricciardulli, L., Foltz, G. R., Manaster, A., & Meissner, T. (2022). Assessment of saildrone extreme wind measurements in Hurricane SAM using MW satellite sensors. *Remote Sensing*, 14(12), 2726. <https://doi.org/10.3390/rs14122726>

Sabine, C., Sutton, A., McCabe, K., Lawrence-Slavas, N., Alin, S., Feely, R., et al. (2020). Evaluation of a new carbon dioxide system for autonomous surface vehicles. *Journal of Atmospheric and Oceanic Technology*, 37(8), 1305–1317. <https://doi.org/10.1175/JTECH-D-20-0010.1>

Schlundt, M., Farrar, J. T., Bigorre, S. P., Plueddemann, A. J., & Weller, R. A. (2020). Accuracy of wind observations from open-ocean buoys: Correction for flow distortion. *Journal of Atmospheric and Oceanic Technology*, 37(4), 687–703. <https://doi.org/10.1175/JTECH-D-19-0132.1>

Susini, S., Menendez, M., Eguia, P., & Blanco, J. M. (2022). Climate change impact on the offshore wind energy over the North Sea and the Irish Sea. *Frontiers in Energy Research*, 10, 881146. <https://doi.org/10.3389/fenrg.2022.881146>

Sutton, A. J., Sabine, C. L., Maenner-Jones, S., Lawrence-Slavas, N., Meinig, C., Feely, R. A., et al. (2014). A high-frequency atmospheric and seawater  $p\text{CO}_2$  data set from 14 open-ocean sites using a moored autonomous system. *Earth System Science Data*, 6(2), 353–366. <https://doi.org/10.3334/CDIAC/OTG.TSM>

Sutton, A. J., Williams, N. L., & Tilbrook, B. (2021). Constraining Southern ocean  $\text{CO}_2$  flux uncertainty using uncrewed surface vehicle observations. *Geophysical Research Letters*, 48(3), e2020GL091748. <https://doi.org/10.1029/2020gl091748>

Takahashi, T., Sutherland, S. C., Wanninkhof, R., Sweeney, C., Feely, R. A., Chipman, D. W., et al. (2009). Climatological mean and decadal change in surface ocean  $p\text{CO}_2$ , and net sea-air  $\text{CO}_2$  flux over the global oceans. *Deep-Sea Research Part II Topical Studies in Oceanography*, 56(8–10), 554–577. <https://doi.org/10.1016/j.dsr2.2008.12.009>

The MathWorks Inc. (2021). MATLAB Version: 9.11.0.2358333 (R2021b) [Software]. The MathWorks Inc. Retrieved from <https://www.mathworks.com>

Thyng, K., Greene, C., Hetland, R., Zimmerle, H., & DiMarco, S. (2016). True colors of oceanography: Guidelines for effective and accurate colormap selection. *Oceanography*, 29(3), 9–13. <https://doi.org/10.5670/oceanog.2016.66>

Wanninkhof, R. (2014). Relationship between wind speed and gas exchange over the ocean revisited. *Limnology and Oceanography: Methods*, 12(JUN), 351–362. <https://doi.org/10.4319/lom.2014.12.351>

Wanninkhof, R., Pickers, P. A., Omar, A. M., Sutton, A., Murata, A., Olsen, A., et al. (2019). A surface ocean  $\text{CO}_2$  reference network, SOCONET and associated marine boundary layer  $\text{CO}_2$  measurements. *Frontiers in Marine Science*, 6, 400. <https://doi.org/10.3389/fmars.2019.00400>

Weiss, R. F. (1974). Carbon dioxide in water and seawater: The solubility of a non-ideal gas. *Marine Chemistry*, 2(3), 203–215. [https://doi.org/10.1016/0304-4203\(74\)90015-2](https://doi.org/10.1016/0304-4203(74)90015-2)

Woolf, D. K. (1997). Bubbles and their role in gas exchange. In *The Sea surface and global change* (1st ed., pp. 173–206). Cambridge University Press. Retrieved from [https://www.cambridge.org/core/product/identifier/CBO9780511525025A013/type/book\\_part](https://www.cambridge.org/core/product/identifier/CBO9780511525025A013/type/book_part)

Zeebe, R., & Wolf-Gladrow, D. (2001).  *$\text{CO}_2$  in seawater: Equilibrium, kinetics, isotopes*. Elsevier Science. Retrieved from <https://books.google.com/books?id=g3j3Zn4kEseC>

Zhang, D., Cronin, M. F., Meinig, C., Thomas Farrar, J., Jenkins, R., Peacock, D., et al. (2019). Comparing air-sea flux measurements from a new unmanned surface vehicle and proven platforms during the spurs-2 field campaign. *Oceanography*, 32(2), 122–133. <https://doi.org/10.5670/oceanog.2019.220>

Zhou, X., Reichl, B. G., Romero, L., & Deike, L. (2023). A sea state dependent gas transfer velocity for  $\text{CO}_2$  unifying theory, model, and field data. *Earth and Space Science*, 10(11), e2023EA003237. <https://doi.org/10.1029/2023EA003237>